RESPONSE TO RC1

We thank the reviewer for the detailed assessment and constructive feedback.
The answers to each comment are detailed below in blue.

This study proposes a novel altimetry-radiometry synergistic approach to improve SMOS thin sea ice thickness (SIT) retrievals by incorporating permittivity estimates derived from CryoSat-2 backscatter observations. By integrating these estimates into a hybrid machine-learning scheme based on an L-band emission model, the authors aim to better constrain sea ice permittivity, which remains a dominant uncertainty source in radiometric retrievals. Validation against independent in situ datasets demonstrates that the synergy of Ku-band altimetry and L-band radiometry yields more physically consistent SIT estimates compared to SMOS-only baselines, particularly for first-year ice. Overall, the manuscript is clear and the proposed framework shows potential for enhancing thin sea ice monitoring for future missions like CIMR and CRISTAL. However, the paper still requires improvements in the following aspects: the simplification of model parameters, the sensitivity of roughness assumptions, and the temporal mismatch between sensors.

General Comments:

1. The SMRT simulation is constructed using three varying parameters (ice temperature, ice salinity, and brine axis ratio), while many other snow and ice parameters are held fixed as background values. This simplification may limit the generalizability of the learned relationships, particularly for pan-Arctic applications where snow and sea ice structure can vary substantially across regions and seasons. The authors are encouraged to further justify these fixed assumptions and discuss their implications for pan-Arctic applicability.

The main concerning assumption is the roughness, particularly that of the snow-ice interface. However, as shown in Figure 3 (of the manuscript), despite different interface roughness (MSS) resulting in various backscatter values, the range between the minimum and maximum values is reasonably maintained. Therefore, its possible effect on the proposed method is mitigated through the backscatter standardization process. Another source of bias could be the large-scale roughness, but its effect is averaged out when regridding the CryoSat-2 measurements into the coarser SMOS grid. In any case, a further analysis has been done and included to study the impact of this large-scale roughness in the simulated backscatter. To quantitatively assess this impact, large-scale roughness has now been integrated into our SMRT modeling via the surface slope (the RMS height of the surface topography). As depicted in Figure R1, an increase in deformation produces a smoothing of the modeled waveform, which results in reduced peak power and lower overall backscatter. This was also done to reproduce the behavior demonstrated in the RC2's SAMOSA+ example. Although the absolute power values show different ranges due to normalization and the distinction between surface slope and surface height standard deviation, the physical response, an increase in roughness producing a reduction in waveform peak power, is consistent between both models. In any case, the range between the maximum and minimum backscatter across the permittivity parameter space (i.e., the axis ratio dependency) remains constant, as further confirmed in Figures R2 and R3. This stability is similar to the effects observed with interface roughness, even considerably less impactful, thus justifying its omission in the current state of the proposed method.

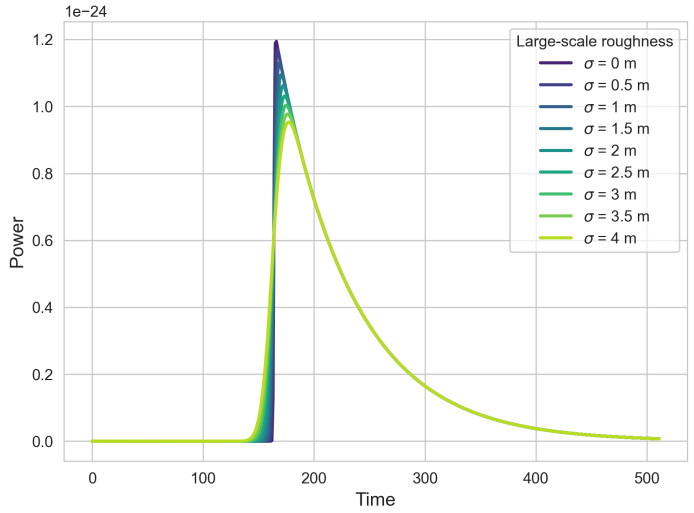

Figure R1. Simulated CryoSat-2 Ku-band waveform across a range of large-scale surface roughness configurations (parameterized via surface slope) using SMRT.

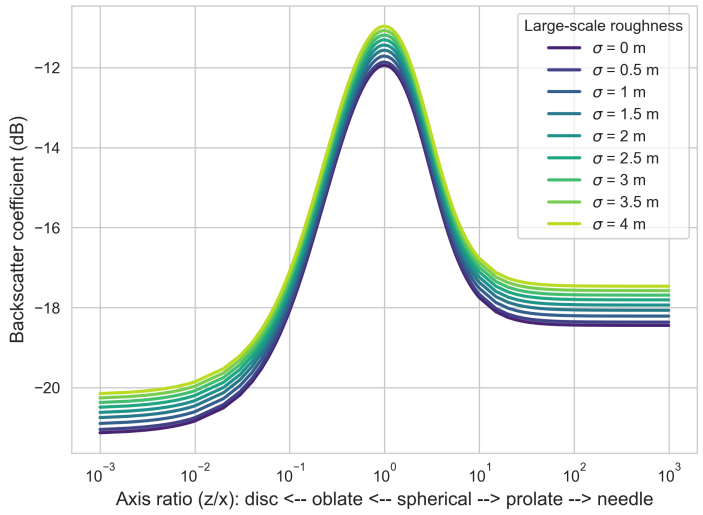

Figure R2. Simulated CryoSat-2 Ku-band backscatter as a function of the sea ice brine inclusion axis ratio across a range of large-scale surface roughness configurations (parameterized via surface slope).

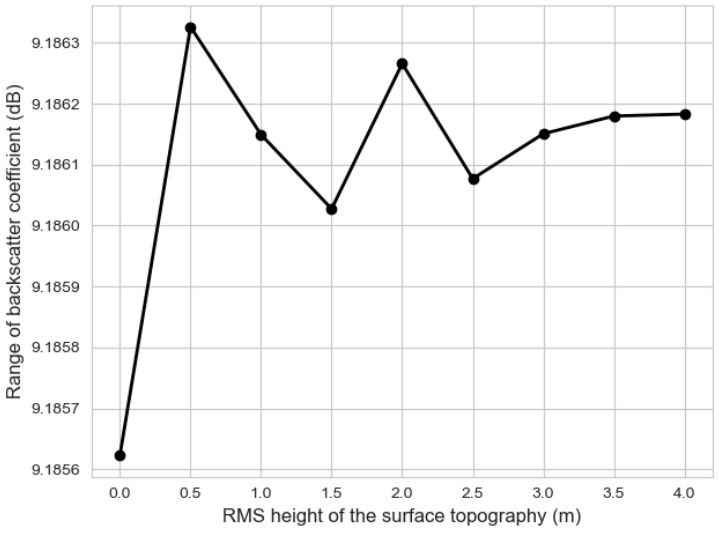

Figure R3. Range (difference between maximum and minimum) of the simulated backscatter as a function of the large-scale roughness.

Other assumptions, such as considering homogeneous snow and ice layers, are built over multiple works and previous works dealing with SIT retrievals that followed this path (Kaleschke et al., 2012; Tian-Kunze et al., 2014; Huntemann et al., 2014; Hernández-Macià et al., 2024), mainly given the difficulty of having knowledge of inner layering within the media.

2. In Section 4.1, the manuscript applies a single MSS = 0.03 to both the air–snow and the snow–ice interfaces in the SMRT. Landy et al. (2020) appears to treat the two interfaces with distinct roughness parameters, while Larue et al. (2021) report a range of MSS values rather than a fixed constant. How sensitive is the SMRT simulation to MSS within a physically plausible range (e.g., consistent with Larue et al., 2021)? And what is the specific rationale for selecting 0.03 here? If MSS is separately prescribed for the air–snow and snow–ice interfaces, how large is the resulting change in simulation results?

A further analysis has been done and included regarding how the simulation output varies with varying roughness in the different interfaces. Furthermore, Landy et al., 2020, states that the air-snow interface roughness is driven by the snow-ice roughness, making our assumption reasonable.

The 0.03 selection is done after an analysis guided by Landy et al., 2020, and Larue et al., 2021, as it is found as an intermediate value (see Figure 3 in the manuscript). While those works also highlight that these interfaces can exhibit distinct roughness distributions (Landy et al., 2020; Larue et al., 2021), utilizing a single parameter in the SMRT simulations might be an advantage while preserving accuracy. Allowing different roughness values for the two interfaces may not yield enhanced results, but it will certainly increase the overall uncertainty budget. However, to further assess the validity of applying a single effective MSS of 0.03 to both the air-snow and snow-ice interfaces, an additional sensitivity test is performed using decoupled roughness parameters.

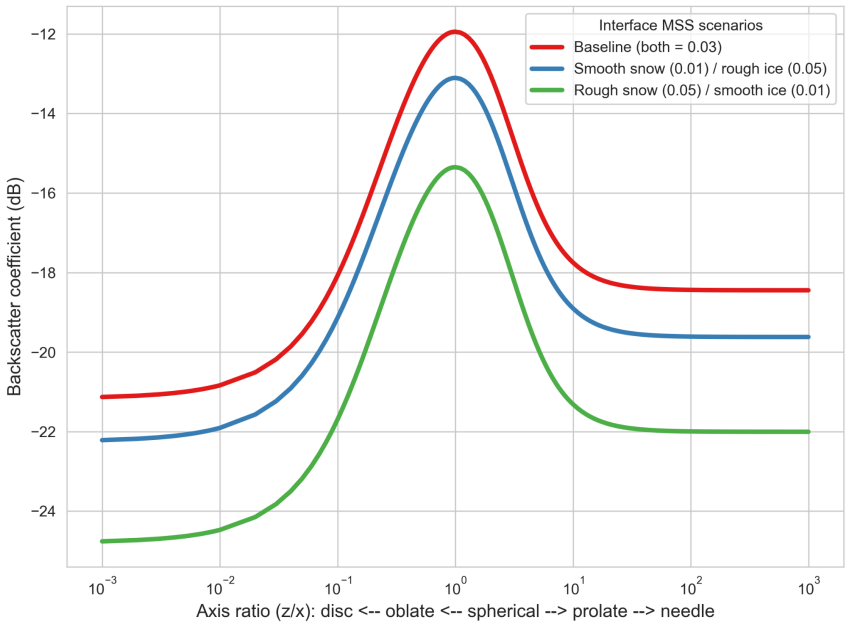

Figure R4. Simulated CryoSat-2 Ku-band backscatter as a function of the sea ice brine inclusion axis ratio for decoupled air-snow and snow-ice MSS parameterizations. The baseline scenario (both interfaces at MSS = 0.03) is compared against configurations with differing roughness combinations.

Figure R4 demonstrates that decoupling the interface roughness produces a shift in the simulated backscatter magnitude. For instance, a rougher air-snow interface (MSS = 0.05) combined with a smoother snow-ice interface (MSS = 0.01) reduces the overall backscatter compared to the reverse configuration. However, the shape of the curve, driven by the brine inclusion shape, remains consistent across all tested scenarios. The baseline configuration (MSS = 0.03) captures this central trend. Furthermore, the range between the minimum and maximum backscatter is well maintained across all configurations, thus not impacting the method after the backscatter scaling process.

3. The proposed synergy combines biweekly averaged CryoSat-2 backscatter with daily SMOS TB, yet the final product is delivered daily. While this temporal mismatch may be unavoidable under current observing constraints, within a 15-day window, ice drift, deformation, and snowfall events could modify scattering conditions, especially in thin-ice or marginal ice zones where ice dynamics are strongest. I encourage the authors to add discussions (and, if feasible, a quantitative assessment) of how this temporal aggregation might impact permittivity estimation and the resulting SIT.

To achieve pan-Arctic coverage and address gaps, the CryoSat-2 measurements aggregated over the 15-day window are regridded to the SMOS grid utilizing a nearest-neighbor interpolation. While we acknowledge that this spatial interpolation might introduce some uncertainty, the 15-day window represents a reasonable trade-off between maximizing spatial coverage and minimizing the effects of sea ice drift. To justify this choice and quantify the impact of both interpolation variance and uncorrected sea ice drift within this time window, we have incorporated a temporal mismatch analysis into the revised manuscript.

To quantitatively assess how this temporal mismatch impacts the retrieved SIT, a first perturbation sensitivity analysis is conducted. Synthetic Gaussian noise ($\sigma = 0.5$) is injected into the standardized CS2 backscatter array within a test dataset (composed of a subset of the training data). This perturbation aims to simulate the variance that ice drift and deformation can induce over a 15-day period. This approach was initially favored over a sea ice drift product given the coarse spatial resolution of such products (62.5 km). The perturbed backscatter is propagated through the RF-eps and RF-synergy models, and the absolute deviation in the predicted thickness (ΔSIT) is evaluated against the baseline prediction. As illustrated in Figure R5, the impact of the temporal mismatch under these synthetic random perturbations is dependent on the ice thickness regime. In the thin-ice domain (<0.25 m), where dynamics are expected to be highest, the deviation in the predicted SIT remains minimal. Conversely, the algorithm exhibits higher sensitivity to the perturbed CS2 data in the medium- and thick-ice regimes. The mean deviation rises, flattening at approximately 0.20 m for ice thicker than 1.0 m. In these domains, the L-band TB is saturated, so the algorithm relies more on the CS2-estimated permittivity. However, thicker pack ice is generally more rigid, exhibiting reduced drift speeds and less change over a two-week period compared to the MIZ. Therefore, while the temporal mismatch is an unavoidable constraint, its impact on the retrieval is minimized by the algorithm's nature.

However, to complement this theoretical assessment and ensure the robustness of the method, the multi-sensor EUMETSAT OSI SAF OSI-405-d sea ice drift product is also utilized. To assess the worst-case scenario, a target date (December 15, 2019) is selected at the end of a 15-day compositing window. The daily displacement vectors from December 1 to 15 are accumulated to

calculate the drift per pixel over this period. This is subsequently utilized to backtrack the spatial coordinates of the satellite measurements, resulting in the extraction of the drift-corrected CS2 radar backscatter, and contrasting it against the “spatially-static” backscatter. The RF-synergy architecture is then evaluated utilizing both inputs to compute the error (ΔSIT) introduced by the ice drift. As demonstrated in Figure R6, the impact of real sea ice drift differs from the theoretical synthetic noise perturbation test. Even under a maximum 15-day temporal shift, the mean drift-induced deviation (dashed red line) remains below 0.005 m across all thickness categories. Furthermore, the interquartile range (IQR) across every regime is less than 0.01 m. This statistical stability is corroborated by the spatial distribution maps in Figure R7. The difference map (Panel c) illustrates that the discrepancies introduced by the temporal lag are minimal across the vast majority of the Arctic pack, with minor differences bounded within ±0.05 m.

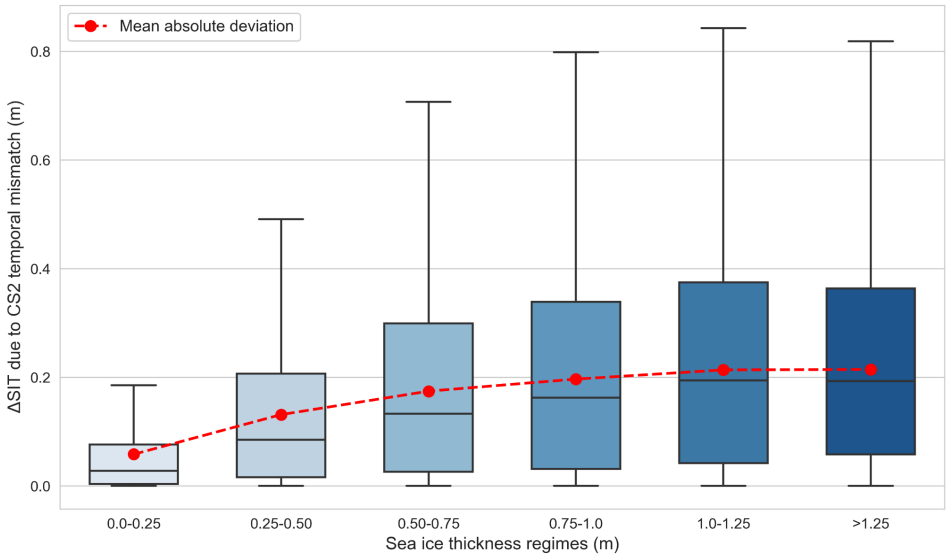

Figure R5. Absolute deviation in the predicted SIT resulting from a simulated 15-day temporal perturbation in the CryoSat-2 backscatter input. The boxplots and mean trendline (red) illustrate the algorithm's varying sensitivity to lagged backscatter data across different baseline thickness regimes.

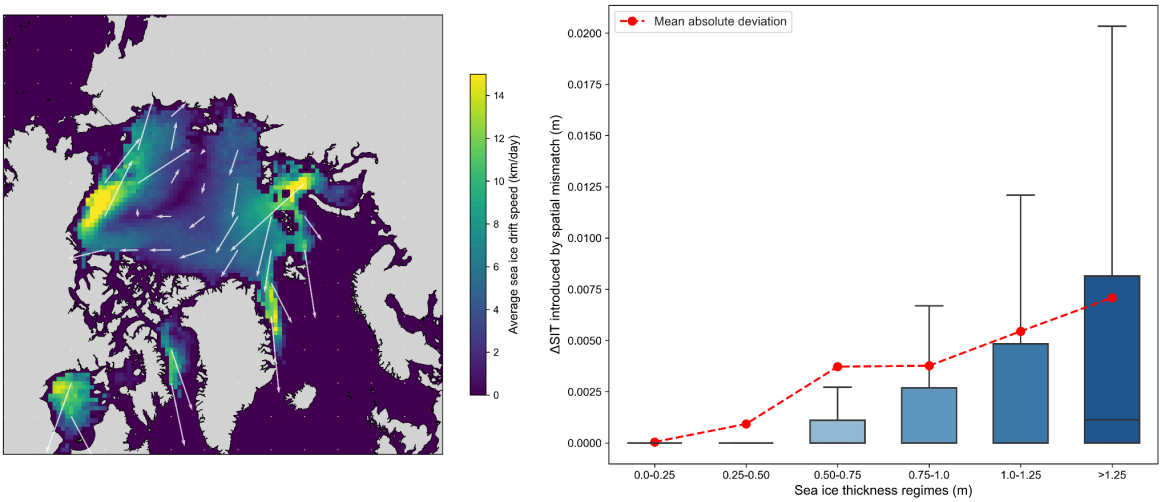

Figure R6. Quantitative assessment of the worst-case temporal mismatch driven by sea ice drift. Left: Full 15-day cumulative sea ice drift speed and direction (December 1-15, 2019) derived from the EUMETSAT OSI SAF OSI-405-d product. Right: Absolute deviation in the predicted SIT resulting from the non-corrected CS2 backscatter. Center lines denote the median, boxes represent the interquartile range (IQR), and the dashed red line indicates the mean drift-induced deviation across thickness regimes.

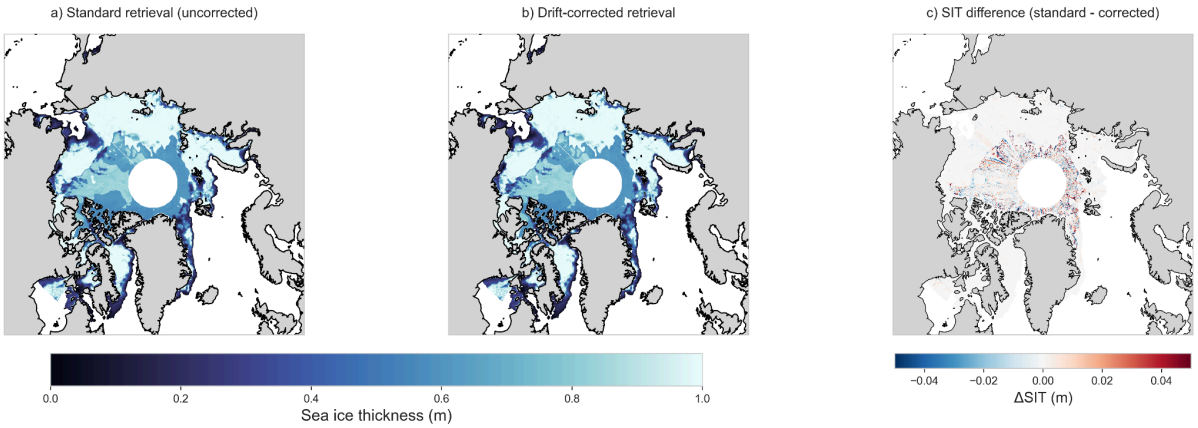

Figure R7. Spatial comparison of the retrieved sea ice thickness for the target date (December 15, 2019). (a) Standard retrieval utilizing the uncorrected, temporally lagged CS2 backscatter. (b) Drift-corrected retrieval utilizing the back-propagated radar data. (c) Spatial difference map.

Specific Comments:

1. In the Abstract, it would be beneficial to include some quantitative results and conclusions to more clearly demonstrate the improvement of the proposed method.

Improved in the manuscript.

2. Lxx (Introduction): The sentence should be revised to: “Despite previous efforts, it remains difficult to determine…”

Corrected in the manuscript.

3. L124, Equation 1: There appears to be a typo here; the bulk ice temperature should be the average of the surface temperature and the seawater temperature.

Corrected in the manuscript.

4. L193-L194: Please add the unit for the salinity; for instance, “…with a fixed temperature and salinity of -10°C and 5 psu.”

The usage of the salinity unit, at least to the authors knowledge, is not standardized anymore and is a matter of debate. In any case, PSUs are dimensionless, so to avoid misunderstandings, salinity is considered unitless in this work.

References

[Hernández-Macià et al., 2024] Hernández-Macià, F., Gabarró, C., Gomez, G. S., & Escorihuela, M. J. (2024). A machine learning approach on SMOS thin sea ice thickness retrieval. *IEEE Journal of Selected Topics in Applied Earth Observations and Remote Sensing, 17*, 10752–10758. https://doi.org/10.1109/JSTARS.2024.3406921

[Huntemann et al., 2014] Huntemann, M., Heygster, G., Kaleschke, L., Krumpen, T., Mäkynen, M., & Drusch, M. (2014). Empirical sea ice thickness retrieval during the freeze-up period from SMOS high incident angle observations. *The Cryosphere, 8*, 439–451. https://doi.org/10.5194/tc-8-439-2014

[Kaleschke et al., 2012] Kaleschke, L., Tian-Kunze, X., Maaß, N., Mäkynen, M., & Drusch, M. (2012). Sea ice thickness retrieval from SMOS brightness temperatures during the Arctic freeze-up period. *Geophysical Research Letters, 39*, L05501. https://doi.org/10.1029/2012GL050916

[Landy et al., 2020] Landy, J. C., Petty, A. A., Tsamados, M., & Stroeve, J. C. (2020). Sea ice roughness overlooked as a key source of uncertainty in CryoSat-2 ice freeboard retrievals. *Journal of Geophysical Research: Oceans, 125*, e2019JC015820. https://doi.org/10.1029/2019JC015820

[Larue et al., 2021] Larue, F., Picard, G., Arnaud, L., Ollivier, A., Delwart, S., … Féménias, P. (2021). Snow Altimetry Radar from ground-based to satellite measurements: Validation of the Snow Microwave Radiative Transfer model (SMRT) in the Alps. *Remote Sensing of Environment, 264*, 112615. https://doi.org/10.1016/j.rse.2021.112534

[Tian-Kunze et al., 2014] Tian-Kunze, X., Kaleschke, L., Maaß, N., Mäkynen, M., Serra, N., Drusch, M., and Krumpen, T.: SMOS-derived thin sea ice thickness: algorithm baseline, product specifications and initial verification, The Cryosphere, 8, 997–1018, https://doi.org/10.5194/tc-8-997-2014, 2014